Available online at www.sciencedirect.com
ScienceDirect
Journal of Computational Physics 227 (2008) 6058–6070
JOURNAL OF COMPUTATIONAL PHYSICS
www.elsevier.com/locate/jcp

Vortex dynamics in complex domains on a spherical surface

Amit Surana [a], Darren Crowdy [b,*]

[a] Department of Mechanical Engineering, Massachusetts Institute of Technology, 77 Massachusetts Avenue, Cambridge, MA 02139, USA
[b] Department of Mathematics, Massachusetts Institute of Technology, 77 Massachusetts Avenue, Cambridge, MA 02139, USA

Received 20 September 2007; received in revised form 9 February 2008; accepted 14 February 2008
Available online 8 March 2008

Abstract

We consider the motion of both point vortices and uniform vortex patches in arbitrary, possibly multiply connected, regions bounded by impenetrable walls on the surface of a sphere. By exploiting knowledge of the functional form of the relevant Green's function in a pre-image circular domain that is conformally equivalent to a stereographic projection of the fluid domain on the spherical surface, we first generalize Kirchhoff–Routh theory for point vortex motion in the plane to point vortex motion on a spherical shell. Next, we study vortex patch motion and show that there is a contour dynamics formulation for the evolution of uniform vortex patches in any finitely connected domain on a spherical shell bounded by impenetrable walls. We describe a novel numerical scheme whereby this motion can be computed. Some illustrative calculations are shown.

Keywords: Vorticity; Contour dynamics; Sphere; Multiply connected

1. Introduction

In planar vortex dynamics, two of the simplest models of vorticity are the point vortex and the uniform vortex patch. The point vortex model has the advantage that the dynamics is reduced to the motion of a (usually finite) set of points but suffers from the disadvantage that it fails to capture any finite-area effects associated with distributed vorticity models. For background on the point vortex problem, see Newton [20]. The vortex patch model, in which regions of vorticity are assumed to be finite-area regions of uniform vorticity, does not suffer from such a drawback [23,22]. Furthermore, owing to the material conservation of vorticity, the dynamics of vortex patches can also be reduced to tracking the motion of the vortex jumps. The associated numerical algorithm has become known as *contour dynamics* [24]. Such numerical algorithms have been extensively studied in the literature. There now exist quite sophisticated manifestations of such codes; for example, *contour surgery* [8,9] implements a method of dealing with the repeated formation of thin vortical filaments in order to facilitate long-time calculations.

* Corresponding author.
E-mail address: crowdy@math.mit.edu (D. Crowdy).

0021-9991/$ - see front matter © 2008 Elsevier Inc. All rights reserved.
doi:10.1016/j.jcp.2008.02.027

These vortex models have predominantly been studied in free space with no solid boundaries present to affect their motion. For many geophysical and astrophysical applications, however, it is crucial to incorporate the effects of coastlines/shorelines on the motion of vortex structures since it is known that such boundaries can greatly influence important dynamical processes such as the global transport of passive tracers like environmental pollutants, biota and heat.

The study of vortex motion in complex, multiply connected domains bounded by impenetrable walls is very much in its infancy. The Hamiltonian structure of the point vortex problem in multiply connected domains was originally pointed out by Lin [17,18]. However, it is only recently that a constructive theory for computing vortex motion in a given domain has appeared: Crowdy and Marshall [2] have found explicit formulae, up to conformal mapping, for the Hamiltonians in fluid regions of arbitrary finite connectivity. These methods have been applied in various circumstances, including the computation of point vortex motion around arrays of circular islands [3] and through gaps in walls [5]. The calculation is facilitated by the fact that the boundary value problem satisfied by the (hydrodynamic) Green's function in the physical domain is conformally invariant and the fact that the functional form for this Green's function in a pre-image circular domain is known [2].

As for point vortex motion in bounded domains on the surface of a sphere, Kidami and Newton [16] have considered this general problem. See also [13]. Their approach relies on the extension of the celebrated "method of images" for planar domains to a spherical surface. As in the planar case, this requires the flow domain to have certain symmetry properties. In contrast, Crowdy [4] employs the technique of conformal mapping to give a more general treatment of the point vortex motion in simply connected domains. The key observation there is that, when boundaries are present, the fluid motion generated by a point vortex does not have to be embedded in a sea of uniform vorticity. This relaxed requirement renders the boundary value problem satisfied by the governing streamfunction conformally invariant. The Hamiltonian for the point vortex motion can then be derived by the explicit knowledge of the Green's function in a pre-image circular domain.

In this paper we extend the conformal mapping approach of Crowdy [4] to study point vortex motion, in multiply connected domains, on the surface of a sphere. By again exploiting the conformal invariance of the boundary value problem satisfied by the Green's function, together with our explicit knowledge of that Green's function for pre-image circular domains [2], we derive a formula which gives a transformation law for the governing Hamiltonian under an arbitrary conformal mapping of the stereographically-projected fluid domain (and, thus, in arbitrary multiply connected domains on the spherical surface). This result provides a generalization of the classical planar Kirchhoff–Routh theory due to Lin [17,18] to point vortex motion in bounded multiply connected domains on a spherical surface. To the best of the authors' knowledge, no such demonstration of the Hamiltonian structure of this problem has previously been given in the literature.

Next, we consider the vortex patch model. In recent work, Crowdy and Surana [7] have shown that there exists a contour dynamics formulation for the motion of vortex patches in arbitrary multiply connected domains in the plane. The key idea is to consider a conformal map to the physical region of interest from a conformally equivalent circular pre-image region. Given this conformal map, the evolution of the pre-image of a given vortex patch is tracked. Here, we extend this formulation to the surface of a sphere. While there are additional terms in the equations associated with the stereographic projection, the contour dynamics formulation remains essentially the same as for planar domains [7]. As a result, the numerical scheme developed in [7] extends in a reasonably straightforward manner to the spherical case. A key advantage of our approach is that it can be applied, in principle, to any multiply connected fluid region on the sphere for which a conformal mapping from a circular pre-image region can be found, either analytically or numerically. Dritschel [9] has already shown how to extend contour dynamics to the surface of a sphere, but does not include the effects of solid walls. A study of the roll-up of strips of vorticity using contour dynamics methods on a spherical surface (again, not including wall effects) has been performed by Dritschel and Polvani [11] with further studies of the dynamics of uniform vortex regions performed later in Polvani and Dritschel [21].

2. Mathematical preliminaries

Let Σ denote a sphere and, without loss of generality, assume the sphere has unit radius. D_Σ will be taken to be an arbitrary multiply connected region (or "basin") with finite connectivity on the surface of Σ. Let

$\{D_j \mid j = 1, \ldots, M\}$ denote $M \geqslant 0$ islands inside D_Σ and let the boundary of D_j be ∂D_j. The outer boundary enclosing the islands is denoted by ∂D_0.

(θ, ϕ) will denote the usual polar and meridional angles in spherical polar coordinates and ∇^2_Σ will be the Laplace–Beltrami operator defined by

$$\nabla^2_\Sigma \equiv \frac{1}{\sin\theta}\frac{\partial}{\partial\theta}\left(\sin\theta\frac{\partial}{\partial\theta}\right) + \frac{1}{\sin^2\theta}\frac{\partial^2}{\partial\phi^2}. \tag{1}$$

The incompressible fluid motion on the surface of Σ can be described by a streamfunction ψ and the local vorticity field ω is related to it via

$$\nabla^2_\Sigma\psi = -\omega. \tag{2}$$

A point vortex solution at some position $(\theta_\alpha, \phi_\alpha)$ on an *unbounded* spherical surface is defined to be the flow given by a streamfunction satisfying

$$\nabla^2_\Sigma\psi(\theta, \phi; \theta_\alpha, \phi_\alpha) = -\delta(\theta, \phi; \theta_\alpha, \phi_\alpha) + \frac{1}{4\pi}. \tag{3}$$

This represents a point vortex embedded in a sea of uniform vorticity. The latter is required to ensure that the total integral of vorticity over the entire spherical shell vanishes. Such a requirement is not relevant for motion in bounded domains since the vorticity field is no longer defined globally on the spherical surface.

In order to consider the case of vortex motion within D_Σ, we introduce the *hydrodynamic Green's function* [12] $G^s(\theta, \phi; \theta_\alpha, \phi_\alpha)$ satisfying

$$\nabla^2_\Sigma G^s(\theta, \phi; \theta_\alpha, \phi_\alpha) = -\delta(\theta, \phi; \theta_\alpha, \phi_\alpha), \quad \text{in } D_\Sigma, \tag{4}$$

with boundary conditions

$$\begin{aligned} &G^s(\theta, \phi; \theta_\alpha, \phi_\alpha) = 0 \quad \text{on } \partial D_0, \\ &G^s(\theta, \phi; \theta_\alpha, \phi_\alpha) = C_j \quad \text{on } \partial D_j, \quad j = 1, \ldots, M. \end{aligned} \tag{5}$$

$\{C_j | j = 1, \ldots, M\}$ is a set of constants independent of (θ, ϕ) (but generally dependent on $(\theta_\alpha, \phi_\alpha)$). These M constants are determined by the M conditions that the circulations around all the enclosed islands are zero, i.e.,

$$\oint_{\partial D_j} \frac{\partial G^s}{\partial n}\mathrm{d}s = 0, \quad j = 1, \ldots, M, \tag{6}$$

where $\partial G^s/\partial n$ is the normal derivative of G^s and $\mathrm{d}s$ is an element of arclength around the boundary of D_Σ.

Let us introduce the stereographic projection of D_Σ onto a region D_z in a complex z plane given by

$$z = \cot(\theta/2)\mathrm{e}^{\mathrm{i}\phi}, \quad z_\alpha = \cot(\theta_\alpha/2)\mathrm{e}^{\mathrm{i}\phi_\alpha}. \tag{7}$$

z_α is the projection of the δ-function singularity. More details of this projection can be found in [1]. We denote the projections of the islands D_j and their boundaries ∂D_j by D^z_j and ∂D^z_j, respectively. This particular choice of projection maps the north pole of the sphere to $z = \infty$; there is another choice which maps the *south* pole to infinity. In some calculations where the vortex motion is predominantly around the regions near the north pole, it may be advantageous to change to this alternative choice. Here, however, we restrict analysis to the z-projection embodied in (7) and do not discuss the matter of swapping coordinate charts (a discussion of related matters can be found in Dritschel [10]).

We will now rewrite $G^s(\theta, \phi; \theta_\alpha, \phi_\alpha)$ as a function of the new independent variables $(z, \bar{z})$. Let this new function be $G^z(z, \bar{z}; z_\alpha, \bar{z}_\alpha)$. It can be shown that (4) takes the form (see [1])

$$(1 + z\bar{z})^2\frac{\partial^2 G^z}{\partial z\partial\bar{z}} = -\delta(z, z_\alpha), \quad \text{in } D_z \tag{8}$$

It is also easy to see that

$$\begin{aligned} &G^z = 0 \quad \text{on } \partial D^z_0, \\ &G^z = C_j \quad \text{on } \partial D^z_j, \quad j = 1, \ldots, M, \end{aligned} \tag{9}$$

with

$$\oint_{\partial D_j^z} \frac{\partial G^z}{\partial n_z} \mathrm{d}s_z = 0, \quad j = 1, \ldots, M. \tag{10}$$

where $\partial G^z/\partial n_z$ is the normal derivative of G^z and $\mathrm{d}s_z$ is an element of arclength around the boundary of the basin in the z-plane of projection.

By an extension of the Riemann mapping theorem [14] it is known that D_z is conformally equivalent to some circular pre-image regions D_ζ consisting of the unit ζ-disc with M smaller circular discs excised. Let C_0 denote the unit disc in a parametric ζ-plane and let $\{C_j \mid j = 1, \ldots, M\}$ be the circular boundaries of the enclosed discs. Let $q_j \in \mathbb{R}$ and $\delta_j \in \mathbb{C}$, respectively, denote the radius and center of the circle C_j. The quantities $\{(\delta_j, q_j) | j = 1, \ldots, M\}$ are known as the *conformal moduli* of the domain D_ζ [19]. Let $z(\zeta)$ be the conformal mapping from the D_ζ to D_z. We will assume that $z(\zeta)$ is known either as an analytical formula or computable by some numerical conformal mapping algorithm.

Let $G^\zeta(\zeta, \overline{\zeta}; \alpha, \overline{\alpha})$ be the relevant hydrodynamic Green's function now in the domain D_ζ. By the conformal invariance of the boundary value problem satisfied by this function, it follows that

$$G^s(\theta, \phi; \theta_\alpha, \phi_\alpha) = G^z(z, \bar{z}; z_\alpha, \bar{z}_\alpha) = G^\zeta(\zeta, \overline{\zeta}; \alpha, \overline{\alpha}), \tag{11}$$

where α is the pre-image of the point z_α in D_ζ under the map $z(\zeta)$, i.e., $z_\alpha = z(\alpha)$. An explicit form for the hydrodynamic Green's function for D_ζ has been found by Crowdy and Marshall [2] and is given by

$$G^\zeta(\zeta, \overline{\zeta}; \alpha, \overline{\alpha}) = -\frac{1}{2\pi} \log \left| \frac{\omega(\zeta, \alpha)}{\alpha \omega(\zeta, \overline{\alpha}^{-1})} \right| = -\frac{1}{4\pi} \log \left(\frac{\omega(\zeta, \alpha)\overline{\omega}(\overline{\zeta}, \overline{\alpha})}{|\alpha|^2 \omega(\zeta, \overline{\alpha}^{-1})\overline{\omega}(\overline{\zeta}, \alpha^{-1})} \right). \tag{12}$$

$\omega(\zeta, \gamma)$ is the so-called *Schottky–Klein prime function* (hereafter denoted SK prime function) associated with D_ζ. One way of defining it is via an infinite product formula (see [2])

$$\omega(\zeta, \gamma) = (\zeta - \gamma)\hat{\omega}(\zeta, \gamma), \tag{13}$$

where

$$\hat{\omega}(\zeta, \gamma) = \prod_{\theta_i \in \Theta''} \frac{(\theta_i(\zeta) - \gamma)(\theta_i(\gamma) - \zeta)}{(\theta_i(\zeta) - \zeta)(\theta_i(\gamma) - \gamma)}, \tag{14}$$

and Θ'' is a set of Möbius maps defined in detail in [2]. It can also be readily computed by a numerical algorithm described by Crowdy and Marshall [6].

3. Kirchhoff–Routh theory on a spherical surface

We first focus on the point vortex problem. Consider fluid motion inside D_Σ which is irrotational except for N moving point vortices with fixed strengths $\{\Gamma_i \mid i = 1, \ldots, N\}$ located at points $\{(\theta_{\alpha_i}, \phi_{\alpha_i}) \mid i = 1, \ldots, N\}$. The streamfunction associated with this system is

$$\psi(\theta, \phi) = \sum_{i=1}^{N} \Gamma_i G^s(\theta, \phi; \theta_{\alpha_i}, \phi_{\alpha_i}). \tag{15}$$

$G^s(\theta, \phi; \theta_{\alpha_i}, \phi_{\alpha_i})$ can be split into a self-induced contribution $G_{pv}(\theta, \phi; \theta_{\alpha_i}, \phi_{\alpha_i})$ and a non-self-induced contribution $\hat{G}^s(\theta, \phi; \theta_{\alpha_i}, \phi_{\alpha_i})$ so that

$$G^s(\theta, \phi; \theta_{\alpha_j}, \phi_{\alpha_j}) = G_{pv}(\theta, \phi; \theta_{\alpha_j}, \phi_{\alpha_j}) + \hat{G}^s(\theta, \phi; \theta_{\alpha_j}, \phi_{\alpha_j}), \tag{16}$$

where

$$G_{pv}(\theta, \phi; \theta_{\alpha_j}, \phi_{\alpha_j}) = -\frac{1}{4\pi} \log \left(\frac{(z - z_{\alpha_j})(\bar{z} - \bar{z}_{\alpha_j})}{(1 + z\bar{z})(1 + z_{\alpha_j}\bar{z}_{\alpha_j})} \right) \tag{17}$$

is the Green's function associated with an isolated point vortex of unit strength on a sphere without boundaries (written in terms of $(z,\bar{z})$). (17) is the solution of Eq. (3). Therefore

$$\begin{aligned}\widehat{G}^s(\theta,\phi;\theta_{\alpha_j},\phi_{\alpha_j}) &= -\frac{1}{4\pi}\log\left(\frac{\omega(\zeta,\alpha_j)\bar{\omega}(\bar{\zeta},\bar{\alpha}_j)}{|\alpha_j|^2\omega(\zeta,\bar{\alpha}_j^{-1})\bar{\omega}(\bar{\zeta},\alpha_j^{-1})}\right)+\frac{1}{4\pi}\log\left(\frac{(z-z_{\alpha_j})(\bar{z}-\bar{z}_{\alpha_j})}{(1+z\bar{z})(1+z_{\alpha_j}\bar{z}_{\alpha_j})}\right),\\ &= -\frac{1}{4\pi}\log\left(\frac{\hat{\omega}(\alpha_j,\alpha_j)\overline{\hat{\omega}}(\bar{\alpha}_j,\bar{\alpha}_j)}{|\alpha_j|^2\omega(\alpha_j,\bar{\alpha}_j^{-1})\bar{\omega}(\bar{\alpha}_j,\alpha_j^{-1})}\right)+\frac{1}{4\pi}\log\frac{(1+z(\alpha_j)\bar{z}(\alpha_j))^2}{|z_\zeta(\alpha_j)|^2}+\mathcal{O}(\zeta-\alpha_j,\bar{\zeta}-\bar{\alpha}_j).\end{aligned} \tag{18}$$

Note first, from (18), the following reciprocity property:

$$\widehat{G}^s(\theta,\phi;\theta_{\alpha_j},\phi_{\alpha_j}) = \widehat{G}^s(\theta_{\alpha_j},\phi_{\alpha_j};\theta,\phi). \tag{19}$$

Second, note that

$$\widehat{G}^s(\theta_{\alpha_j},\phi_{\alpha_j};\theta_{\alpha_j},\phi_{\alpha_j}) = -\mathcal{R}(\alpha_j,\bar{\alpha}_j)+\frac{1}{2\pi}\log\frac{|z_\zeta(\alpha_j)|}{(1+z(\alpha_j)\bar{z}(\alpha_j))}, \tag{20}$$

where

$$\mathcal{R}(\alpha_j,\bar{\alpha}_j) \equiv \frac{1}{4\pi}\log\left(\frac{\hat{\omega}(\alpha_j,\alpha_j)\overline{\hat{\omega}}(\bar{\alpha}_j,\bar{\alpha}_j)}{|\alpha_j|^2\omega(\alpha_j,\bar{\alpha}_j^{-1})\bar{\omega}(\bar{\alpha}_j,\alpha_j^{-1})}\right). \tag{21}$$

$\mathcal{R}(\alpha_j,\bar{\alpha}_j)$ is sometimes referred to as the Robin function [2] for the point vortex motion in the ζ domain. Now, the motion of the jth point vortex on a sphere is governed by the equations

$$\dot{\theta}_{\alpha_j} = \frac{1}{\sin\theta_{\alpha_j}}\frac{\partial\psi^j(\theta,\phi)}{\partial\phi}\bigg|_{\theta_{\alpha_j},\phi_{\alpha_j}}, \quad \dot{\phi}_{\alpha_j} = -\frac{1}{\sin\theta_{\alpha_j}}\frac{\partial\psi^j(\theta,\phi)}{\partial\theta}\bigg|_{\theta_{\alpha_j},\phi_{\alpha_j}}, \tag{22}$$

where, $\psi^j(\theta,\phi)$ is the non-self-induced streamfunction

$$\psi^j(\theta,\phi) = \sum_{i=1}^{N}{}' \Gamma_i G^s(\theta,\phi;\theta_{\alpha_i},\phi_{\alpha_i}) + \Gamma_j\widehat{G}^s(\theta,\phi;\theta_{\alpha_j},\phi_{\alpha_j}). \tag{23}$$

Here, the notation $\sum_{i=1}^{N}{}'$ indicates a sum over i between 1 and N but disallowing $i=j$. Note that, for any j

$$\begin{aligned}\frac{\partial\widehat{G}^s(\theta,\phi;\theta_{\alpha_i},\phi_{\alpha_i})}{\partial\phi}\bigg|_{\theta_{\alpha_j},\phi_{\alpha_j}} &= \frac{1}{2}\frac{\partial\widehat{G}^s(\theta_{\alpha_j},\phi_{\alpha_j};\theta_{\alpha_j},\phi_{\alpha_j})}{\partial\phi_{\alpha_j}},\\ \frac{\partial\widehat{G}^s(\theta,\phi;\theta_{\alpha_i},\phi_{\alpha_i})}{\partial\theta}\bigg|_{\theta_{\alpha_j},\phi_{\alpha_j}} &= \frac{1}{2}\frac{\partial\widehat{G}^s(\theta_{\alpha_j},\phi_{\alpha_j};\theta_{\alpha_j},\phi_{\alpha_j})}{\partial\theta_{\alpha_j}},\end{aligned} \tag{24}$$

where, we have used the reciprocity (19) of $\widehat{G}^s$. Hence (22) can be expressed as

$$\dot{\theta}_{\alpha_j} = \frac{1}{\sin\theta_{\alpha_j}}\frac{\partial\Psi^j(\{\theta_{\alpha_i}\},\{\phi_{\alpha_i}\})}{\partial\phi_{\alpha_j}}, \quad \dot{\phi}_{\alpha_j} = -\frac{1}{\sin\theta_{\alpha_j}}\frac{\partial\Psi^j(\{\theta_{\alpha_j}\},\{\phi_{\alpha_i}\})}{\partial\theta_{\alpha_j}}, \tag{25}$$

where we define

$$\Psi^j(\{\theta_{\alpha_j}\},\{\phi_{\alpha_i}\}) = \sum_{i=1}^{N}{}'\Gamma_i G^s(\theta_{\alpha_j},\phi_{\alpha_j};\theta_{\alpha_i},\phi_{\alpha_i}) + \frac{\Gamma_j}{2}\widehat{G}^s(\theta_{\alpha_j},\phi_{\alpha_j};\theta_{\alpha_j},\phi_{\alpha_j}). \tag{26}$$

Introducing the canonical change of variables

$$P_j = \cos\theta_{\alpha_j}, \quad Q_j = \phi_{\alpha_j}, \tag{27}$$

(25) becomes

$$\dot{P}_j = -\frac{\partial \overline{\Psi}^j(\{P_i\},\{Q_i\})}{\partial Q_j}, \quad \dot{Q}_j = \frac{\partial \overline{\Psi}^j(\{P_i\},\{Q_i\})}{\partial P_j}, \tag{28}$$

$$\overline{\Psi}^j(\{P_i\},\{Q_i\}) \equiv \Psi^j(\{\cos^{-1} P_i\},\{Q_i\}). \tag{29}$$

Hence, N vortex motion in a multiply connected domain on a sphere is a Hamiltonian dynamical system with

$$\Gamma_j \dot{Q}_j = \frac{\partial H^s(\{Q_i\},\{P_i\})}{\partial P_j}, \quad \Gamma_j \dot{P}_j = -\frac{\partial H^s(\{Q_i\},\{P_i\})}{\partial Q_j}, \tag{30}$$

and $H^s(\{P_i\},\{Q_j\})$ given by

$$H^s(\{Q_i\},\{P_i\}) = \frac{1}{2}\sum_{j=1}^{N}\sum_{i=1}^{N}{}' \Gamma_j \Gamma_i G^s(\cos^{-1} P_j, Q_j; \cos^{-1} P_i, Q_i) + \frac{1}{2}\sum_{j=1}^{N} \Gamma_j^2 \widehat{G}^s(\cos^{-1} P_j, Q_j; \cos^{-1} P_j, Q_j)$$

where we have again used the reciprocity (19) of G^s. Using (11) and (20) in above relation we get

$$\begin{aligned} H^s(\{Q_i\},\{P_i\}) &= \frac{1}{2}\sum_{j=1}^{N}\sum_{i=1}^{N}{}' \Gamma_j \Gamma_i G^\zeta(\alpha_j,\bar{\alpha}_j;\alpha_i,\bar{\alpha}_i) - \frac{1}{2}\sum_{j=1}^{N}\Gamma_j^2 \mathcal{R}(\alpha_j;\bar{\alpha}_j) + \frac{1}{4\pi}\sum_{j=1}^{N}\Gamma_j^2 \log\frac{|z_\zeta(\alpha_j)|}{(1+z(\alpha_j)\bar{z}(\alpha_j))}, \\ &= H^\zeta(\{\alpha_i\}) + \frac{1}{4\pi}\sum_{j=1}^{N}\Gamma_j^2 \log\frac{|\, z_\zeta(\alpha_j)\,|}{(1+z(\alpha_j)\bar{z}(\alpha_j))}, \\ &= H^z(\{z_{\alpha_i}\}) + \frac{1}{4\pi}\sum_{j=1}^{N}\Gamma_j^2 \log\frac{1}{(1+z(\alpha_j)\bar{z}(\alpha_j))} \end{aligned} \tag{31}$$

where $H^\zeta(\{\alpha_i\})$ and $H^z(\{z_{\alpha_i}\})$ denote the point vortex Hamiltonians in the ζ and z domains, respectively.

The important point to note is that the Hamiltonians governing N vortex motion on the surface of the sphere are not invariant under either stereographic projection or conformal mapping. They do, however, have simple transformation rules, embodied in (31). Formula (31) generalizes, to the surface of a sphere, similar formulae given by Lin [17,18] for the Hamiltonians governing N point vortex motion in conformally equivalent multiply connected planar domains.

3.1. Examples

We can now compute point vortex trajectories in some example domains. Consider a non-uniform channel bounded by the northern hemisphere and a cap at the south pole. The resulting domain is doubly connected. The stereographic projection of this fluid domain i.e. D_z, is conformally equivalent to an annulus $q < |\zeta| < 1$ under the conformal map

$$z(\zeta) = \frac{\zeta - \alpha}{|\,\alpha\,|\,(\zeta - \alpha^{-1})}, \tag{32}$$

for appropriate values of $\alpha \in \mathcal{C}$ and $q \in \mathbf{R}^+$. The vortex trajectories exhibit two different behaviours: those starting close to the upper or lower boundary of the channel encircle the channel; those starting in the middle of the channel are closed though they do not encircle the channel (see Fig. 1).

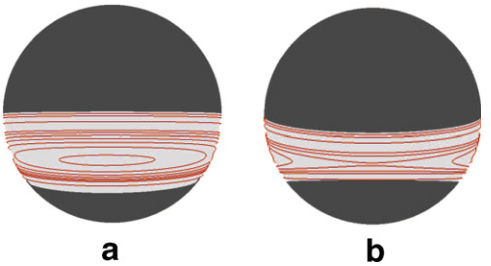

Fig. 1. Two different views of point vortex trajectories in a non-uniform channel.

Fig. 2. Point vortex trajectories in a basin with two islands.

Fig. 2 shows a similar calculation when there are two obstacles in a basin so the domain is now triply connected. It should be clear that calculations in domains of any finite connectivity are similarly possible with no additional difficulty. For geometrically interesting domains, conformal mappings from multiply connected circular pre-image regions are needed.

4. Vortex patch dynamics in bounded domains on a sphere

In this section we now consider fluid motion inside D_Σ which is irrotational except for a time-evolving vortex patch P_s of uniform vorticity ω_0. We shall denote the stereographic projection of P_s on the z-plane by P_z and the conformal pre-image of P_z by P_ζ. Let ∂P_s, ∂P_z and ∂P_ζ denote the respective patch boundaries.

The streamfunction ψ corresponding to the velocity field induced by the patch P_s on the sphere satisfies

$$\nabla^2_\Sigma \psi = \begin{cases} -\omega_0, & (\theta,\phi) \in P_s, \\ 0 & \text{otherwise}, \end{cases} \tag{33}$$

with same boundary conditions as given earlier for G^s. In terms of G^s, ψ can be expressed as (see [7] for details)

$$\psi(\theta,\phi) = \omega_0 \int\int_{P_s} G^s(\theta,\phi;\theta_\alpha,\phi_\alpha)\mathrm{d}S(\theta_\alpha,\phi_\alpha). \tag{34}$$

Using the fact that the area element $\mathrm{d}S = \sin\theta \mathrm{d}\theta\mathrm{d}\phi$ on the sphere and the area element $dxdy = (\mathrm{d}\bar{z}\wedge\mathrm{d}z)/2i$ on the stereographic plane are related by

$$\mathrm{d}S = \frac{4}{(1+z\bar{z})^2}\frac{\mathrm{d}\bar{z}\wedge\mathrm{d}z}{2i}, \tag{35}$$

together with the scaling relation

$$\mathrm{d}\bar{z}\wedge\mathrm{d}z = |z'(\zeta)|^2 \mathrm{d}\bar{\zeta}\wedge\mathrm{d}\zeta, \tag{36}$$

and invoking the conformal invariance (11), we obtain

$$\begin{aligned}\psi(\theta,\phi) &= \omega_0 \int\int_{P_s} G^s(\theta,\phi;\theta_\alpha,\phi_\alpha)\mathrm{d}S(\theta_\alpha,\phi_\alpha), = \omega_0 \int\int_{P_z} G^z(z,\bar{z};z_\alpha,\bar{z}_\alpha)\frac{4}{(1+z_\alpha\bar{z}_\alpha)^2}\frac{\mathrm{d}\bar{z}_\alpha\wedge\mathrm{d}z_\alpha}{2i}, \\ &= \frac{\omega_0}{2i}\int\int_{P_\zeta} G^\zeta(\zeta,\bar{\zeta};\alpha,\bar{\alpha})\frac{4z'(\alpha)\bar{z}'(\bar{\alpha})}{(1+z(\alpha)\bar{z}(\bar{\alpha}))^2}\mathrm{d}\bar{\alpha}\wedge\mathrm{d}\alpha. \end{aligned} \tag{37}$$

The fluid velocity field (u_θ, u_ϕ) can be determined from the stream function ψ as

$$u_\phi - \mathrm{i}u_\theta = \frac{2z}{\sin\theta}\frac{\partial\psi^z}{\partial z} = \frac{2z(\zeta)}{z'(\zeta)\sin\theta}\frac{\partial\Psi}{\partial\zeta}\bigg|_{\bar{\zeta}}, \tag{38}$$

where

$$\sin\theta = \frac{2\sqrt{z(\zeta)\bar{z}(\zeta)}}{1+z(\zeta)\bar{z}(\zeta)}, \tag{39}$$

$$\psi^z(z,\bar{z}) = \psi(\theta(z,\bar{z}),\phi(z,\bar{z})), \quad \Psi(\zeta,\bar{\zeta}) = \psi^z(z(\zeta),\bar{z}(\bar{\zeta})), \tag{40}$$

$$\left.\frac{\partial \Psi}{\partial \zeta}\right|_{\bar{\zeta}} = -\frac{\omega_0}{8\pi \mathrm{i}} \int\int_{P_\zeta} \left(\frac{\omega_\zeta(\zeta,\alpha)}{\omega(\zeta,\alpha)} - \frac{\omega_\zeta(\zeta,\bar{\alpha}^{-1})}{\omega(\zeta,\bar{\alpha}^{-1})} \right) \frac{4z'(\alpha)\bar{z}'(\bar{\alpha})}{(1+z(\alpha)\bar{z}(\bar{\alpha}))^2} \mathrm{d}\bar{\alpha} \wedge \mathrm{d}\alpha$$

$$= -\frac{\omega_0}{8\pi \mathrm{i}} \int\int_{P_\zeta} \frac{\partial}{\partial \bar{\alpha}} \left(-\frac{\omega_\zeta(\zeta,\alpha)}{\omega(\zeta,\alpha)} \frac{4z'(\alpha)}{(1+z(\alpha)\bar{z}(\bar{\alpha}))z(\alpha)} \right) \mathrm{d}\bar{\alpha} \wedge \mathrm{d}\alpha$$

$$+ \frac{\omega_0}{8\pi \mathrm{i}} \int\int_{P_\zeta} \frac{\partial}{\partial \alpha} \left(-\frac{\omega_\zeta(\zeta,\bar{\alpha}^{-1})}{\omega(\zeta,\bar{\alpha}^{-1})} \frac{4\bar{z}'(\bar{\alpha})}{(1+z(\alpha)\bar{z}(\bar{\alpha}))\bar{z}(\bar{\alpha})} \right) \mathrm{d}\bar{\alpha} \wedge \mathrm{d}\alpha$$

$$= -\frac{\omega_0}{8\pi \mathrm{i}} \int\int_{P_\zeta} \frac{\partial}{\partial \bar{\alpha}} \left(\frac{\omega_\zeta(\zeta,\alpha)}{\omega(\zeta,\alpha)} F(\alpha,\bar{\alpha}) \right) \mathrm{d}\bar{\alpha} \wedge \mathrm{d}\alpha + \frac{\omega_0}{8\pi \mathrm{i}} \int\int_{P_\zeta} \frac{\partial}{\partial \alpha} \left(\frac{\omega_\zeta(\zeta,\bar{\alpha}^{-1})}{\omega(\zeta,\bar{\alpha}^{-1})} \overline{F}(\bar{\alpha},\alpha) \right) \mathrm{d}\bar{\alpha} \wedge \mathrm{d}\alpha$$

and we have introduced the function

$$F(\alpha,\bar{\alpha}) = -\frac{4z'(\alpha)}{(1+z(\alpha)\bar{z}(\bar{\alpha}))z(\alpha)}. \tag{41}$$

Invoking the complex form of Stokes theorem (twice) we finally obtain

$$\left.\frac{\partial \Psi}{\partial \zeta}\right|_{\bar{\zeta}} = -\frac{\omega_0}{8\pi \mathrm{i}} \left[\int_{\partial P_\zeta} \left(\frac{\omega_\zeta(\zeta,\alpha)}{\omega(\zeta,\alpha)} F(\alpha,\bar{\alpha}) \right) \mathrm{d}\alpha + \int_{\partial P_\zeta} \left(\frac{\omega_\zeta(\zeta,\bar{\alpha}^{-1})}{\omega(\zeta,\bar{\alpha}^{-1})} \overline{F}(\bar{\alpha},\alpha) \right) \mathrm{d}\bar{\alpha} \right]. \tag{42}$$

This last equation shows that the calculation of the velocity field outside the patch P_s reduces to the evaluation of a line integral. This means there is a contour dynamics formulation for the evolution of a uniform vortex patch in any finitely connected domain on a sphere.

An important observation is that the line integrals appearing in (42) are exactly of the same form as those arising in the contour dynamics formulation in planar domains as presented in [7]; the only difference is that, in the planar case, the function F is instead given by

$$F(\alpha,\bar{\alpha}) = z'(\alpha)\bar{z}(\bar{\alpha}). \tag{43}$$

With this observation the numerical algorithm developed for contour dynamics in planar domains with impenetrable boundaries [7] extends to the spherical case in a straightforward manner, as described in the next section.

4.1. Contour dynamics algorithm for sphere

We now outline the three key steps in our contour dynamics algorithm. The method is an adaptation of that already presented in Crowdy and Surana [7]. Many of the ideas to follow are borrowed from Dritschel [8,9] but have been adapted for present purposes.

1. *Contour representation and adaptive node adjustment.* Following Dritschel [8] we represent the contour ∂P_s by a set of nodes with the spherical coordinates (θ_k, ϕ_k) and use interpolating functions between them. Let $\mathbf{x}_j = (\cos\phi_j \sin\theta_j, \sin\phi_j \sin\theta_j, \cos\theta_j)$ be the corresponding Cartesian coordinates for the node j then the contour between two nodes say $\mathbf{x}_j$ and $\mathbf{x}_{j+1}$ is assumed to take the form

$$\mathbf{X}_j(s) = \mathbf{x}_i + s(\mathbf{x}_{j+1} - \mathbf{x}_j) + \eta_j(s)(\mathbf{x}_j \times \mathbf{x}_{j+1}) + \frac{1}{4} s(1-s)(\mathbf{x}_{j+1} + \mathbf{x}_j) \mid \mathbf{x}_{j+1} - \mathbf{x}_j|^2, \tag{44}$$

where

$$\eta_j(s) = \alpha_j s + \beta_j s^2 + \gamma_j s^3, \tag{45}$$

for $0 \leqslant s \leqslant 1$. The coefficients in $\eta(s)$ are

$$\alpha_j = -\frac{1}{3} e_j \kappa_j - \frac{1}{6} e_j \kappa_j, \quad \beta_j = \frac{1}{2} e_j \kappa_j, \quad \gamma_j = \frac{1}{6} e_j (\kappa_{j+1} - \kappa_j), \tag{46}$$

where $e_j = \mid \mathbf{x}_{j+1} - \mathbf{x}_j \mid$ and κ_j is the curvature given by

$$\kappa_j = \frac{2\mathbf{x}_j \cdot (\mathbf{x}_+ \times \mathbf{x}_-)}{|\,\mathbf{x}_+ e_-^2 - \mathbf{x}_- e_+^2\,|}, \tag{47}$$

with

$$\mathbf{x}_\pm = \mathbf{x}_{j\pm1} - \mathbf{x}_j, \quad e_\pm = |\,\mathbf{x}_\pm\,|\,. \tag{48}$$

The algorithm for adaptive node adjustment is the same as for the planar case treated in [7] with the value of curvature used being the total curvature $\sqrt{\kappa_j^2 + 1}$.

2. *Evaluation of contour integrals on the sphere.* To evaluate expression (42) we split the integrals as

$$\left.\frac{\partial \Psi}{\partial \zeta}\right|_{\bar\zeta} = I_r(\zeta) + I_s(\zeta), \tag{49}$$

where

$$I_r(\zeta) = -\frac{\omega_0}{8\pi \mathrm{i}}\left[\oint_{\partial P_\zeta} \frac{\overline{F}(\bar\alpha,\alpha)}{(\zeta - \bar\alpha^{-1})}\mathrm{d}\bar\alpha + \oint_{\partial P_\zeta}\left(\frac{\hat\omega_\zeta(\zeta,\alpha)}{\hat\omega(\zeta,\alpha)}F(\alpha,\bar\alpha)\right)\mathrm{d}\alpha + \oint_{\partial P_\zeta}\left(\frac{\hat\omega_\zeta(\zeta,\bar\alpha^{-1})}{\hat\omega(\zeta,\bar\alpha^{-1})}\overline{F}(\bar\alpha,\alpha)\right)\mathrm{d}\bar\alpha\right], \tag{50}$$

and

$$I_s(\zeta) = \frac{\omega_0}{8\pi \mathrm{i}}\oint_{\partial P_\zeta}\frac{F(\alpha,\bar\alpha)}{(\alpha-\zeta)}\mathrm{d}\alpha. \tag{51}$$

The contour ∂P_ζ in D_ζ domain is represented by a set of image nodes under the conformal map, i.e. $\{\zeta_j \mid j = 1,\ldots,N\}$ with a locally-determined cubic polynomial as the interpolation function. In this scheme, the contour between two nodes ζ_j and ζ_{j+1} is represented by

$$\beta_j(s) = \zeta_i + s(\zeta_{j+1} - \zeta_j) + \mathrm{i}\eta_j(s)(\zeta_{j+1} - \zeta_j), \tag{52}$$

where, $e_j = |\,\zeta_{j+1} - \zeta_j\,|$, $\eta_j(s)$ is given by (45) and κ_j is the planar curvature at node ζ_j computed by passing a circle through the nodes ζ_{j-1}, ζ_j and ζ_{j+1}. With the cubic representation of contour (44), the contour integral (50) becomes

$$\begin{aligned} I_r(\zeta) = & -\frac{\omega_0}{8\pi\mathrm{i}}\sum_{j=1}^{N}\int_0^1 \frac{\overline{F}(\bar\beta_j(s),\beta_j(s))}{(\zeta-\beta_j(\bar s)^{-1})}\bar\beta_j'(s)\mathrm{d}s - \frac{\omega_0}{8\pi\mathrm{i}}\sum_{j=1}^{N}\int_0^1\left(\frac{\hat\omega_\zeta(\zeta,\beta_j(s))}{\hat\omega(\zeta,\beta_j(s))}F(\beta_j(s),\overline{\beta}_j(s))\right)\beta_j'(s)\mathrm{d}s \\ & -\frac{\omega_0}{8\pi\mathrm{i}}\sum_{j=1}^{N}\int_0^1\left(\frac{\hat\omega_\zeta(\zeta,\bar\beta_j^{-1}(s))}{\hat\omega(\zeta,\bar\beta_j^{-1}(s))}\overline{F}(\bar\beta_j(s),\beta_j(s))\right)\bar\beta_j'(s)\mathrm{d}s. \end{aligned}$$

Since for a nodal point i.e., $\zeta = \zeta_k$, the integrals appearing in I_r remain regular, $I_r(\zeta_k)$ can be computed using any standard numerical quadrature scheme. Computation of $I_s(\zeta)$ at $\zeta = \zeta_k$, however requires care. The integral can be expressed as

$$I_s(\zeta_k) = \frac{\omega_0}{8\pi\mathrm{i}}\sum_{j=1,j\neq k-1,k}^{N}\int_0^1\frac{F(\beta_j(s),\bar\beta_j(s)) - F(\zeta_k,\bar\zeta_k)}{(\beta_j(s)-\zeta_k)}\beta_j'(s)\mathrm{d}s + I_{k-1}(\zeta_k) + I_k(\zeta_k), \tag{53}$$

where

$$I_k(\zeta_k) \approx \frac{\omega_0}{8\pi\mathrm{i}}\left[\frac{\partial F(\zeta_k,\bar\zeta_k)}{\partial\alpha}(\zeta_{k+1}-\zeta_k) + \frac{\partial F(\zeta_k,\bar\zeta_k)}{\partial\bar\alpha}(\bar\zeta_{k+1}-\bar\zeta_k)(1-\mathcal{I}_k)\right], \tag{54}$$

$$I_{k-1}(\zeta_k) \approx \frac{\omega_0}{8\pi\mathrm{i}}\left[\frac{\partial F(\zeta_k,\bar\zeta_k)}{\partial\alpha}(\zeta_k-\zeta_{k-1}) + \frac{\partial F(\zeta_k,\bar\zeta_k)}{\partial\bar\alpha}(\bar\zeta_k-\bar\zeta_{k-1})(1-\mathcal{I}_{k-1})\right], \tag{55}$$

with

$$\begin{aligned} \frac{\partial F(\zeta_k,\bar\zeta_k)}{\partial\alpha} &= -\frac{4z_{\zeta\zeta}(\zeta_k)}{(1+z(\zeta_k)\bar z(\bar\zeta_k))z(\zeta_k)} + \frac{4z_\zeta^2(\zeta_k)}{(1+z(\zeta_k)\bar z(\bar\zeta_k))z^2(\zeta_k)} + \frac{4z_\zeta^2(\zeta_k)\bar z(\bar\zeta_k)}{(1+z(\zeta_k)\bar z(\bar\zeta_k))^2 z(\zeta_k)}, \\ \frac{\partial F(\zeta_k,\bar\zeta_k)}{\partial\bar\alpha} &= \frac{4|z_\zeta(\zeta_k)|^2}{(1+z(\zeta_k)\bar z(\bar\zeta_k))^2}, \end{aligned} \tag{56}$$

and

$$\mathcal{I}_k = 2\int_0^1 \ln(1 + \mathrm{i}[\alpha_k + \beta_k s + \gamma_k s^2])\mathrm{d}s, \quad \mathcal{I}_{k-1} = 2\int_0^1 \ln(1 - \mathrm{i}\alpha_{k-1} s + \mathrm{i}\gamma_{k-1} s^2])\mathrm{d}s. \tag{57}$$

The integrals $\mathcal{I}_{k-1}$ and $\mathcal{I}_k$ can be computed analytically but we omit the details here.

3. *Advection of the contour.* The patch boundary ∂P_s position is updated by advecting each node (θ_k, ϕ_k), $k = 1, \ldots, N$ in time. The evolution of a node satisfies the ordinary differential equation

$$\dot{\theta}_k = u_\theta(\theta_k, \phi_k), \quad \dot{\phi}_k = \frac{1}{\sin\theta_k} u_\phi(\theta_k, \phi_k), \tag{58}$$

where the velocity components (u_θ, u_ϕ) are given by the relation (38). We use an explicit fourth-order Runge–Kutta scheme for the time-stepping.

5. Numerical examples

The current implementation of our algorithm is a basic one meant to examine the viability of the new scheme in practice. It performed well in a series of test cases in the planar case [7] and we now present some similar examples on a spherical surface. Since we do not perform contour surgery, we do not expect that our current numerical implementation of the algorithm to be able to perform integrations over very long times. As a result, we are not able to show the evolution of the patch once filamentation becomes significant. A future manifestation of the code should incorporate such contour surgery procedures.

5.1. A spherical cap

Consider a spherical surface with a solid circular cap covering the north pole of the sphere. Suppose the cap corresponds in z plane of projection to the circular disc $D_z = \{|\, z \,| \leqslant r_0\}$. D_z is conformally equivalent to the unit disc under the simple conformal map

$$z(\zeta) = r_0\zeta. \tag{59}$$

This example has been studied both by Kidambi and Newton [16] and Crowdy [4] for the case of point vortices and, as expected, the point vortex trajectories are found to be concentric circles coinciding with the latitude circles of the sphere. On the other hand, Fig. 3 shows snapshots of the evolution of a vortex patch. Like the point vortex trajectories, the patch path also encircles the spherical cap, irrespective of its initial location. This is evident from Fig. 3a and b for which the patch is initialized near the equator and Fig. 3c and d for which the patch is released near the cap. However, note that when the patch starts off nearer to the cap, it begins to develop long thin filamentary strands (see Fig. 3d). This is expected since, being near the solid wall, the patch experiences large strain rates from the image vorticity in the wall. This is qualitatively similar to what is observed in the planar case for the patch near an infinite straight wall [7]. It is reassuring, however, that the current algorithm captures the onset of filamentation with no difficulty.

5.2. Motion through a gap in wall

Consider the problem of vortex patch motion through a gap in a wall. For the plane, the problem was considered first by Johnson and McDonald [15]. Suppose there exists an impenetrable wall around the great circle corresponding to $\phi = 0, \pi$ except for a single gap symmetrical about the south pole, spanning the latitudes $[\pi - \theta_0, \pi]$ where θ_0 is some chosen angle between 0 and π. In the z plane of projection the wall corresponds to the segment of the real axis

$$(-\infty, -L) \cup (L, \infty), \tag{60}$$

where, $L = \cot\theta_0/2$ and the conformal map to the unit disc is given by

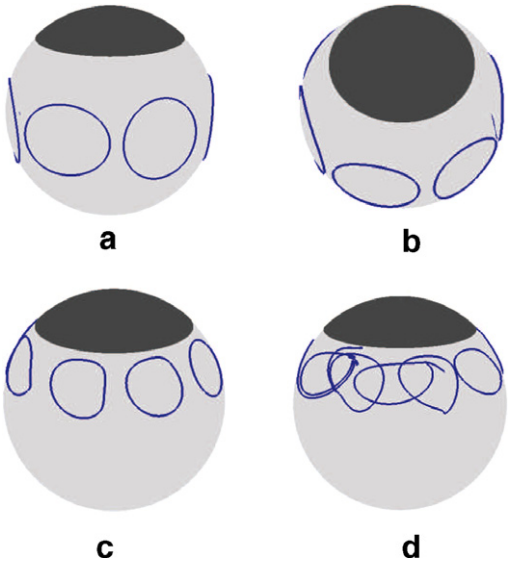

Fig. 3. Vortex patch evolution in a region exterior to a spherical cap with boundary at latitude $\theta_0 = \frac{\pi}{4}$. The four figures show the evolution as the initial patch is initially increasingly close to the wall. Eventually, a filamentary thread is seen to form.

$$z(\zeta) = \frac{2L\zeta}{1+\zeta^2}. \tag{61}$$

Depending on the value of θ_0 (or equivalently, L), qualitatively different point vortex trajectories can arise [4]. Concerning vortex patch motion we consider two values of $\theta_0 = \pi/2$ $(L = 1)$ and $\theta_0 = 3\pi/4$ $(L = 0.4142)$ leading to two different types of behaviour: Fig. 4 shows the patch evolution for $L = 1$, while Fig. 5a and b show the two possible qualitatively distinct patch motions for $L = 0.4142$. For $L = 1$, we take the initial position of the patch to be far from the wall; it does not undergo filamentation as it encircles the wall (see Fig. 4a and b for two different views of patch evolution). On the other hand, the initial location of the patch in Fig. 5a is sufficiently close to the wall that the patch undergoes filamentation as it moves around it.

5.3. Multiply connected domains

The domains in the examples considered so far have been simply connected and the SK prime function is just $\omega(\zeta,\gamma) = (\zeta - \gamma)$. To apply the method to a domain of higher connectivity, all that is needed is to modify this prime function to incorporate the topological differences associated with higher connected domains. This simplicity is one of the main advantages of the method.

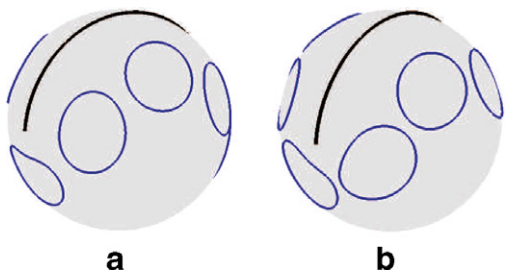

Fig. 4. Two different views of the evolution of a vortex patch near a gap in a wall for gap-width corresponding to $L = 1$. For this initial condition, the patch passes through the gap.

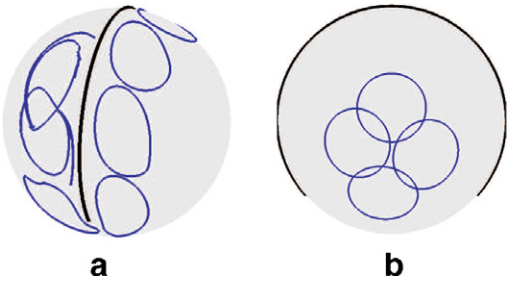

Fig. 5. Two qualitatively different types of vortex patch evolution for a gap-width corresponding to $L = 0.4142$: (a) the patch encircles the wall; (b) the patch evolves along a closed path confined to one side to the wall.

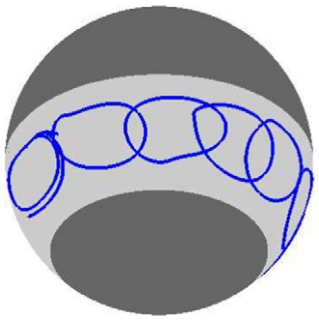

Fig. 6. Vortex patch evolution in a uniform channel. This domain is doubly connected. The onset of filamentation is clearly seen.

Consider the case of a doubly connected fluid domain – vortex motion in a channel encircling the spherical surface. The circular domain D_ζ can now be taken as the concentric circular annulus $\rho < |\zeta| < 1$ and the relevant SK prime function (obtained from the infinite product formulae (13) and (14)) in this case is

$$\omega(\zeta,\gamma) = C\gamma^{-1}P(\zeta\gamma^{-1}) \tag{62}$$

where C is an unimportant constant and

$$P(\zeta) = (1-\zeta)\prod_{k=1}^{\infty}(1-\rho^{2k}\zeta)(1-\rho^{2k}\zeta^{-1}). \tag{63}$$

As found in the case of a point vortex, a vortex patch moves in a uniform channel in a circular path as shown in Fig. 6. Note, however, that finite-area effects now play a role: filamentation is seen to occur as the patch gets closer to the two boundary walls since it experiences the high strain rates associated with the image vorticity in the walls.

6. Conclusion

In this paper, by using an approach based on conformal mapping, we have extended Kirchhoff–Routh theory in a constructive way to multiply connected domains on a spherical shell and derived an explicit formula for the Hamiltonian governing the motion of N point vortices. Further, it has been shown that there exists a contour dynamics formulation for the evolution of uniform vortex patches in any such multiply connected domain on a spherical surface. The algorithm is similar to an analogous contour dynamics scheme, relevant to planar multiply connected domains, presented recently by Crowdy and Surana [7]. The numerical implementation presented here is a straightforward extension of that method. The efficacy of the numerical scheme has been demonstrated through a series of examples.

The method is very general and can be combined with any existing numerical conformal mapping code to compute the point vortex and vortex patch motion in more or less arbitrary flow domains on a sphere. Our

current numerical implementation is not optimal, however, and can be improved in various ways. This includes incorporating contour surgery procedures to allow integrations over longer times; a second possibility is to find improved ways to compute the integrals involved in the velocity calculations to higher order accuracy. These challenges are left for the future.

Acknowledgments

DGC acknowledges support from a 2004 Philip Leverhulme Prize in Mathematics, an EPSRC Advanced Research Fellowship and partial support from the European Science Foundation's MISGAM and HCAA projects. He also acknowledges the hospitality of the Department of Mathematics at MIT where this research was carried out.

References

[1] D.G. Crowdy, M. Cloke, Analytical solutions for distributed multipolar vortex equilibria on a sphere, Phys. Fluids 15 (2003) 22.
[2] D.G. Crowdy, J.S. Marshall, Analytical formulae for the Kirchoff–Routh path function in multiply connected domains, Proc. R. Soc. A 461 (2005) 2477–2501.
[3] D.G. Crowdy, J.S. Marshall, The motion of a point vortex around multiple circular islands, Phys. Fluids 17 (2005) 056602.
[4] D.G. Crowdy, Point vortex motion of surface of a sphere with impenetrable boundaries, Phys. Fluids 18 (2006) 036602.
[5] D.G. Crowdy, J.S. Marshall, The motion of a point vortex through gaps in walls, J. Fluid Mech. 551 (2006) 31–48.
[6] D.G. Crowdy, J.S. Marshall, Computing the Schottky–Klein prime function on the Schottky double of planar domains, Comput. Meth. Funct. Theory 7 (1) (2007) 293–308.
[7] D.G. Crowdy, A. Surana, Contour dynamics in complex domains, J. Fluid Mech. 593 (2007) 235–254.
[8] D.G. Dritschel, Contour surgery: a topological reconnection scheme for extended integrations using contour dynamics, J. Comp. Phys. 77 (1988) 240–266.
[9] D.G. Dritschel, Contour dynamics/surgery on the sphere, J. Comp. Phys. 79 (1988) 477–483.
[10] D.G. Dritschel, A fast contour dynamics method for many-vortex calculations in two-dimensional flows, Phys. Fluids 5 (1) (1993) 173–186.
[11] D.G. Dritschel, L.M. Polvani, The roll-up of vorticity strips on the surface of a sphere, J. Fluid Mech. 234 (1992) 47–69.
[12] M. Flucher, B. Gustafsson, Vortex Motion in Two Dimensional Hydrodynamics, TRITA-MAT-1997-MA 02, Royal Institute of Technology, Stockholm, 1997.
[13] E. Gutkin, P.K. Newton, The method of images and Green's function for spherical domains, J. Phys. A: Math. Gen. 37 (2004) 11989–12003.
[14] G.M. Goluzin, Geometric Theory of Functions of a Complex Variable, AMS Monographs, AMS, 1959.
[15] E.R. Johnson, N.R. McDonald, The motion of a vortex near a gap in a wall, Phys. Fluids 16 (2) (2004) 462–469.
[16] R. Kidambi, P.K. Newton, Point vortex motion on a sphere with solid boundaries, Phys. Fluids 12 (2000) 581–588.
[17] C.C. Lin, On the motion of vortices in two dimensions I: existence of the Kirchhoff–Routh function, Proc. Nat. Acad. Sci. 27 (1941) 570–575.
[18] C.C. Lin, On the motion of vortices in two dimensions II: some further investigations of the Kirchhoff–Routh function, Proc. Nat. Acad. Sci. 27 (1941) 575–577.
[19] Z. Nehari, Conformal Mapping, Dover, New York, 1952.
[20] P.K. Newton, The *N*-vortex Problem, Springer-Verlag, New York, 2001.
[21] L.M. Polvani, D.G. Dritschel, Wave and vortex dynamics on the surface of a sphere, J. Fluid Mech. 255 (1993) 35–64.
[22] D.I. Pullin, Contour dynamics methods, Ann. Rev. Fluid Mech. 24 (1992) 89–115.
[23] P.G. Saffman, Vortex Dynamics, Cambridge University Press, Cambridge, 1992.
[24] N.J. Zabusky, M.H. Hughes, K.V. Roberts, Contour dynamics for the Euler equations in two dimensions, J. Comput. Phys. 30 (1979) 96.